Journal of Quantitative Spectroscopy & Radiative Transfer 112 (2011) 1420–1428

Contents lists available at ScienceDirect

Journal of Quantitative Spectroscopy & Radiative Transfer

journal homepage: www.elsevier.com/locate/jqsrt

60-GHz oxygen band: Precise experimental profiles and extended absorption modeling in a wide temperature range

D.S. Makarov [a,*], M.Yu. Tretyakov [a], P.W. Rosenkranz [b]

[a] IAP RAS, Uljanova str. 46, 603950 Nijniy Novgorod, Russia
[b] Massachusetts Institute of Technology, Cambridge, MA 02139, USA

ARTICLE INFO

Article history:
Received 13 January 2011
Received in revised form
24 February 2011
Accepted 26 February 2011
Available online 3 March 2011

Keywords:
Microwave spectroscopy
Collisional coupling
Absorption model
Atmosphere
Molecular oxygen

ABSTRACT

The 60-GHz band of atmospheric oxygen was studied in the temperature range of −28° to +60 °C at atmospheric pressure by means of a resonator spectrometer with absorption-variation sensitivity of 0.002 dB/km. The experimental data obtained have sufficient signal-to-noise ratio to take second-order mixing into account, increasing the accuracy of the millimeter-wave propagation model (MPM). A refined set of mixing coefficients for the model is derived from the new data and presented. The fidelity of the new model to the spectrometer data is generally better than 2% between 54 and 65 GHz.

1. Introduction

Accurate information on the absorption of radiation in the atmosphere is in demand for atmospheric applications, wireless communications, remote sensing, etc. The main atmospheric absorbers of microwave radiation are water vapor and molecular oxygen. In the millimeter-wave range, widely used for the aforementioned applications, molecular oxygen has a strong band between 50 and 70 GHz and a single spectral line at 118.75 GHz. The absorption band near 60 GHz and the line at 118.75 GHz are formed by magnetic-dipole transitions between fine-structure energy levels within the $^3\Sigma$ electronic ground state of the oxygen molecule. Due to electronic spin, each rotational level of the oxygen molecule is split into a spin triplet corresponding to the three possible space orientations of the total electronic spin vector **S**. If **N** is rotational angular momentum, then the resultant angular momentum is $\mathbf{J}=\mathbf{N}+\mathbf{S}$. Due to symmetry reasons only odd rotational quantum numbers N are allowed for the principal isotopologue, $^{16}O_2$. Since for the oxygen molecule spin $S=1$, possible values for the total angular momentum quantum number J are $N+1$, N, $N-1$. The selection rule $\Delta J=\pm 1$ leaves only two series of lines: $J'\leftarrow J=N\leftarrow N+1$ (usually denoted as $N+$ lines) and $J'\leftarrow J=N\leftarrow N-1$ ($N-$lines). Also, the diagonal matrix elements of the magnetic dipole are nonzero, which leads to a non-resonant absorption due to collisional reorientation (classical approach to this phenomenon is given in [1]). Other transitions, with nonzero ΔN, appear at submillimeter wavelengths. At one-atmosphere pressure all $N+$ and $N-$ lines, except the isolated $1-$ line at 118.75 GHz, blend together and form a wide band ranging from 50 to 70 GHz. Because of the mixing effect, the resulting intensity differs from a simple sum of Van Vleck–Weisskopf profiles [1] of isolated lines.

Theoretical and experimental studies of the band have a long history, beginning in the first half of the twentieth century [2,3]. General theoretical expressions for the shape of the bands formed by overlapping lines were developed in [4,5]. For the 60-GHz molecular-oxygen band, a model considering the mixing effect to first-order

* Corresponding author.
E-mail address: dmak@appl.sci-nnov.ru (D.S. Makarov).

0022-4073/$ - see front matter © 2011 Elsevier Ltd. All rights reserved.
doi:10.1016/j.jqsrt.2011.02.018

in pressure was suggested in [6], and, later, a more thorough description with extension to second-order was given in [7].

Extensive laboratory studies resulted in the development of an accurate millimeter-wave propagation model (MPM) [8] and its further improvement in [9]. The most recent update includes line central frequencies and half-widths measured in [10] and line amplitudes from the HITRAN database [11]. MPM uses a first-order mixing model for millimeter-wave oxygen spectra, where mixing coefficients are derived by the method given in [12].

The present study continues our series of papers (see [13] and references therein) related to the microwave spectrum of molecular oxygen in the atmosphere. In [10] it was shown that the experimental record of the band systematically deviates from the first-order MPM prediction. The objective of this study is to develop a second-order 60-GHz absorption-band model based on precise experimental profiles, to increase modeling accuracy for atmospheric applications.

2. Experiment

The band absorption profile was recorded by means of a resonator spectrometer with fast digital frequency scanning [14]. To allow measurements over a wide temperature range, the resonator was setup in the climate chamber equipped with cooling and heating elements, described in [13]. As in [13,14], gas temperature was measured by a set of temperature sensors with the measurement accuracy 0.1 °C; gas pressure was measured by means of a calibrated pressure meter (600–800 mmHg range), providing measurement accuracy ± 0.5 mmHg.

The absorption coefficient of the gas sample in the chamber is obtained at the frequency points corresponding to eigen-frequencies of the resonator, and its value is calculated from the directly measured Fabry–Perot resonance width:

$$\alpha(f_k) = \frac{2\pi}{c}(\Delta f - \Delta f_0) \quad (1)$$

where α is the absorption coefficient, f_k is the k-th resonator eigen-frequency, Δf and Δf_0 are Fabry–Perot resonance widths measured in air and in pure nitrogen (having negligibly small absorption in the millimeter-wave range), respectively.

In comparison to experiments in [13], the resonator length L was decreased to 39.4 cm to avoid noticeable increase of diffraction losses at lower frequencies [15]. For resonator length of 39.4 cm and mirror diameter 14 cm, one-pass losses (the total relative losses of radiat ion energy during one traversal of the resonator) due to diffraction at 45 GHz (the lowest frequency where absorption was measured) are not greater than 10^{-5}. Since both baseline losses in the chamber filled by pure nitrogen and the total losses in the chamber filled with air are measured, diffraction losses are not considered in experimental data processing because they are canceled by subtraction of the baseline from the total resonator losses [14]. However, lower diffraction losses lead to a narrower resonance–response curve, which is directly measured in the experiment. It is important to decrease resonance-curve width because a wider response curve implies greater measurement errors.

With resonator length of 39.4 cm, intermode distance calculated as $c/2L$ is equal to 380.71 MHz. That allows about 100 points (eigen-frequencies of the resonator) for absorption measurements in the frequency range between 45 and 85 GHz. While running the measurements, gas temperature and humidity, as well as the resonator mirror temperatures, were recorded to take into account their fluctuations in experimental data processing as discussed in [10].

The band absorption profile was recorded at various temperature values in the range of 245–334 K. Gas losses, total resonator losses and baseline signal, recorded at 303 K, are shown in Fig. 1 as a typical example. Several absorption profiles obtained at various temperatures are shown in Fig. 2, demonstrating variation of the band profile with temperature within the studied range.

We decided to use outdoor atmospheric air as a sample for the experiment. This air contains water vapor which gives additional absorption in the millimeter- and submillimeter-wave range. Also, at low temperatures moist air causes hoar-frost on the resonator parts, so the air should be dehydrated before being directed into the climatic chamber. For dehydration, the outdoor air, pumped by an air compressor, was led through a pipe immersed in

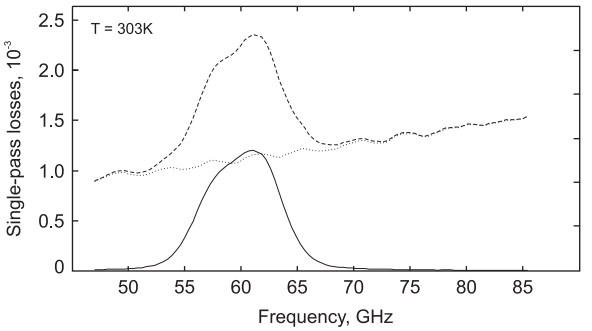

Fig. 1. Loss profiles at 303 K: total losses (dash line), baseline (dotted line) and gas losses (solid line).

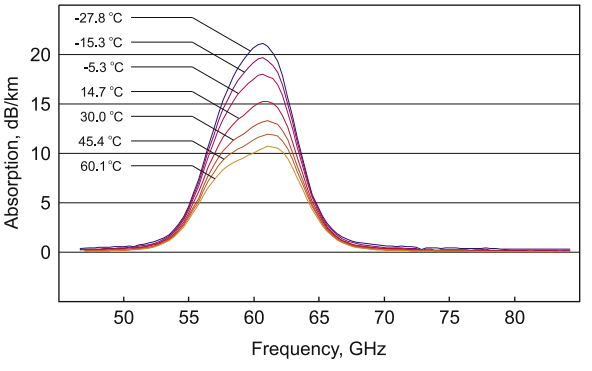

Fig. 2. Absorption profiles in air at several temperatures.

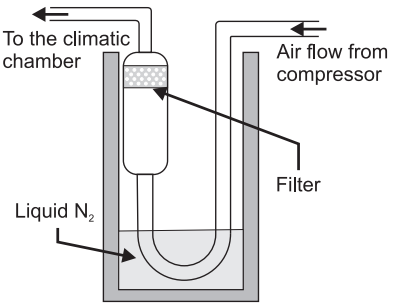

Fig. 3. Diagram of the cold trap.

a Dewar with liquid nitrogen, followed by a dense air filter to remove frosted water from the air flow (see Fig. 3).

Oxygen's condensation temperature is slightly higher than liquid-nitrogen temperature, and if cooling of the air flow is too strong (which happens if the level of liquid nitrogen in the Dewar is high), the oxygen concentration value may decrease due to condensation. As the nitrogen evaporates and the level gets low, the air pipe becomes warmer and condensed oxygen also evaporates, which leads to an increase of oxygen concentration which may even exceed the standard value of 21%. To prevent large concentration deviations, the level of liquid nitrogen in the Dewar was kept close to an experimentally determined optimal value during the band-profile recording. Despite the measures taken, oxygen concentration in the air used for the experiment still varied in the range of 20–21% from one experimental profile record to another. The reason might be variation of the oxygen concentration in the atmosphere. Weak concentration fluctuations within each record were also possible because of small variations of the air flow and the liquid-nitrogen level. Deviation of concentration within the range of 1% gives a noticeable deviation of the profile magnitude, but negligible deviation of the profile shape. The average oxygen concentration value for each profile record was determined by fitting of the MPM profile magnitude to the experimental one. Concentration values thus obtained were taken into account in the mixing-coefficient calculation described below.

The spectrometer had an absorption-variation sensitivity of 0.002 dB/km; but for various reasons discussed in [14], including subtraction of a baseline, small temperature gradients within the spectrometer, etc., the noise level of the experimental profiles was ~ 0.01 dB/km for the lowest absorption values (it increased near the band center, as discussed below). Still, this noise level was several times smaller than in [10]. This decrease of the noise level was achieved by using a reference microwave synthesizer with lower phase noise in comparison to the one used in [10], and by better stability of gas temperature and humidity in the chamber during the experiment.

3. Data treatment

Considering line mixing to second-order in pressure, the absorption profile is described by the following expression [7]:

$$\alpha(f)=\sum_i C_i f^2\left(\frac{\Delta\nu_i\cdot(1+g_iP^2)+Y_i\cdot(f-\nu_i-\delta\nu_iP^2)}{\Delta\nu_i^2+(f-\nu_i-\delta\nu_iP^2)^2}+\frac{\Delta\nu_i\cdot(1+g_iP^2)-Y_i\cdot(f+\nu_i+\delta\nu_iP^2)}{\Delta\nu_i^2+(f+\nu_i+\delta\nu_iP^2)^2}\right) \quad (2)$$

where the sum is over all lines in the band, i is the individual line index, f is the frequency of measurement, C_i is the line amplitude, $\Delta\nu_i$ is the line half-width at half maximum, ν_i is the line central frequency, and Y_i is the first-order mixing parameter; $\Delta\nu_i$ and Y_i are proportional to pressure P: $\Delta\nu_i=\gamma_i\cdot P$, $Y_i=y_i\cdot P$, where γ_i is the broadening coefficient and y_i is the first-order mixing coefficient. The g_i and $\delta\nu_i$ are second-order mixing coefficients accounting for mixing of line intensities and line central frequencies, respectively. The non-resonant component of absorption is included in the summation as $i=0$, with $\nu_0=0$, $Y_0=0$, $g_0=0$ and $\delta\nu_0=0$. Eq. (2) assumes that no first-order line shift is present, which has been confirmed by measurements of oxygen at low pressures [10]. (Eq. (2) has been corrected for a sign error in Eq. (17) of [7]; it is evident from Eqs. (10) and (A17) of [7] that $\delta\nu_i$ should bear the same sign as ν_i in Eq. (2).) The coefficients y_i, g_i and $\delta\nu_i$ are all related, by Eqs. (15), (16) and (19) in [7], to combinations of elements of a line-space collisional-relaxation matrix **w**. Those equations are based on the binary-collision approximation, in which **w** is multiplied by the gas pressure; the terms of first- and second-order in pressure in Eq. (2) derive from a perturbation expansion of the way in which the lines combine through mixing. The temperature dependence of the coefficients, on the other hand, is not easily obtainable from that analysis, so in this work we use an empirical model to fit the experimentally determined temperature dependence of the mixing coefficients.

In [10] it was shown that analysis of the band shape taking only first-order mixing into account (i.e., setting $g_i=0$ and $\delta\nu_i=0$) gives a residual which is regular and looks like a second-order mixing contribution. The noise level of absorption measurements in [10] was 0.05 dB/km, and this value was insufficient for taking the next order of mixing into account, while the current noise level of 0.01 dB/km allows it. Fig. 4 shows the calculated contribution due to the second-order mixing effect, using coefficients from [7] (dotted line) together with two residuals between experimental data at room temperature (300 K) and MPM considering only the

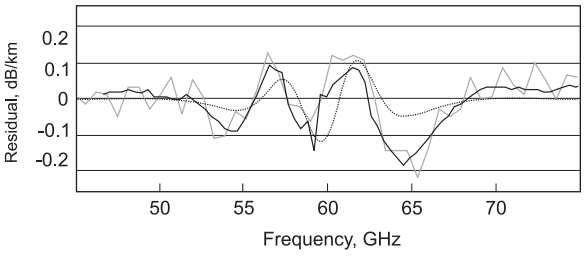

Fig. 4. Experiment-minus-model residual error using first-order mixing models from [10] (gray line) and this work at 300 K (solid black line). Dotted line: theoretical contribution of second-order mixing.

first-order mixing effect. The first residual (gray) is derived from earlier experimental data [10], the second one (black) is derived from the latest data with lower noise level. Because the introduction of second-order mixing coefficients makes the estimation problem nonlinear, we used an iterative algorithm to derive both first- and second-order mixing coefficients from the new experimental data.

If we consider the n strongest lines (current model uses $n=19$) in each branch of the oxygen fine-structure spectrum, then the dimensions of the line-space matrix $\mathbf{w}$ are $6n\times 6n$, with two series of lines ($N+$ and $N-$) at the positive frequencies v_i, two series at $-v_i$, and two series at $v_0=0$ [16]. Negative-frequency lines correspond to the second term within the brackets of Eq. (2). The overlap of the positive-frequency lines with the zero- and negative-frequencies is minimal and therefore can be modeled well by a first-order treatment, which results in a small, though not negligible, bias value b_i to be included in y_i [6,12]. The b_i have values of approximately $-0.014\ \mathrm{bar}^{-1}$ for an effective (i.e., post-mixing) non-resonant broadening coefficient $\gamma_0=0.56$ GHz/bar (bar$=10^5$ Pa).

Now we define an intra-branch collisional-relaxation matrix, which is an $n\times n$ submatrix of $\mathbf{w}$, and assume that it applies identically to all six sets of lines in $\mathbf{w}$. As discussed in [12], to calculate mixing coefficients we need to specify only half of this submatrix, as the other half is related by the constraint of detailed balancing. The diagonal elements are equal to the line-broadening coefficients, which were measured in [10]. Conceptually, we can arrange the elements of the upper-right off-diagonal triangle of the intra-branch submatrix as a vector $\mathbf{r}$. This vector is estimated by the Twomey–Tikhonov method, which implies minimization of the quantity

$$\sum_k \varepsilon_k^2+q\beta \tag{3}$$

where ε_k is the difference between measured and calculated absorption at frequency f_k, $q=\mathbf{r}^\top\cdot\mathbf{H}\cdot\mathbf{r}$ is a quadratic measure of structure in the collisional-relaxation matrix, and β is a Lagrange multiplier which can be chosen to balance between minimal residuals and minimal relaxation-matrix structure [12]. Superscript $\top$ denotes the transpose. Very small β can reduce residuals, but the derived mixing coefficients then do not have a smooth dependence on the quantum number N, which conflicts with theoretical assumptions. Methods for selecting the most suitable value of β are discussed in detail in [12,10]. The solution for $\mathbf{r}$ is [12]

$$\mathbf{r}=\mathbf{H}^{-1}\mathbf{K}^\top\mathbf{V}^\top(\mathbf{V}\mathbf{K}\mathbf{H}^{-1}\mathbf{K}^\top\mathbf{V}^\top+\beta\cdot I)^{-1}\mathbf{A} \tag{4}$$

with

$$A_k=(\alpha_k^{meas}-\alpha_k^{bias})/s_k \tag{5}$$

where α_k^{meas} is the absorption measured at frequency f_k, α_k^{bias} is the absorption calculated by setting $Y_i=b_i\cdot P$ in Eq. (2), and the pre-whitening factor s_k is discussed below; matrices $\mathbf{H}$ and $\mathbf{K}$ are defined in [12] and

$$V_{ki}=\frac{P}{s_k}\frac{\partial\alpha(f_k)}{\partial Y_i} \tag{6}$$

In each iteration of the estimation algorithm, $\mathbf{r}$ is estimated by using the g_i and δv_i values derived in the previous iteration to calculate α_k^{bias} (on the first iteration, the second-order coefficients are set to zero). The vector $\mathbf{y}$ of first-order coefficients is given by $\mathbf{y}=\mathbf{K}\cdot\mathbf{r}+\mathbf{b}$. Then new second-order mixing coefficients are calculated using the $\mathbf{r}$ obtained in the current iteration, considering intra-branch mixing only. These iterations were repeated until the calculated mixing coefficients converged to consistent values from iteration to iteration.

Note that the previously measured [10] broadenings γ_i, as well as the coefficients y_i, g_i and δv_i calculated in the present work, are pressure-independent by definition and Eq. (2) allows one to process the band profile recorded at any particular pressure. The pressure value was measured and used as a parameter in the model profile (2), which makes possible precise quantitative characterization of pressure-dependent effects

Rather than using a fixed value of β, we found that convergence improved if β/m, where m is the number of measurement points, was set to a relatively high value near unity for the first seven iterations and then gradually lowered to an asymptotic value, e.g.:

$$\beta=\begin{cases}1.05\cdot m, & \eta\le 7\\ (0.05+2^{7-\eta})\cdot m, & 7\le\eta\le 20\end{cases} \tag{7}$$

where η is the iteration number.

The Twomey–Tikhonov method provides a solution that fits the measurements within a certain residual-error level, but it is not a unique solution. With $\beta=0.05m$, the $\beta\cdot\mathbf{I}$ term in the denominator of Eq. (4) dominates all but about four or five of the eigenvalues of the denominator matrix. Hence there are effectively about four to five degrees of freedom in $\mathbf{r}$, although it contains $n(n\text{-}1)/2=171$ elements for $n=19$. It is therefore important to distinguish between the uncertainty of the calculated absorption, and uncertainties in the values of the model's coefficients. The coefficients are adjusted to fit measurements, and underestimation of some coefficients can be counterbalanced by excess values in other coefficients when absorption is calculated. However, we consider the set of mixing coefficients finally obtained here as providing the best fidelity of the model to the whole set of experimental profiles as well as corresponding to theoretical principles.

As in [10], an error-model function was used to pre-whiten the data, decreasing the weight of points in the center of the band where measurement errors were higher. This is discussed in the following section. We also accounted for other isotopologues of O_2 by multiplying the calculated absorption by 1.0053 [10]. Unlike the procedure in [10], we do not use any previous version of $\mathbf{y}$ as a baseline here, because g_i and δv_i are calculated from $\mathbf{r}$, not from an incremental change to it.

4. Discussion

In Fig. 5, experiment-minus-model residuals for the absorption profile treated by the model including both

first- and second-order mixing, in comparison to residuals for a model based on only first-order mixing [10], are shown for several temperatures by the black and gray lines, respectively. In this figure, residuals shown by the solid black lines were calculated with the pre-whitening factor s_k set to unity. The dotted lines will be discussed later. Systematic discrepancies between the extended model and experiment are still noticeable, especially at lower temperatures, where the mixing effect should be stronger. These discrepancies are similar for records repeated at the same experimental conditions, so they are not caused by random experimental errors. Nevertheless, in general, the extended model gives smaller residuals in the temperature range considered. In particular, residuals decreased in the frequency bands from 53 to 56 GHz and from 63 to 66 GHz. The lower of these two bands is of special importance because it is widely used for atmospheric sensing (see, e.g., [17]).

One notices that the residuals have some features near the center of the band which look like strong noise peaks. Two reasons leading to appearance of the features are possible. The first is a general increase of the measurement error due to the growth of the resonator response-curve width with increase of the radiation losses in the gas. The second reason is the aforementioned possible deviation of the oxygen concentration due to dehydration of the air used for the experiment, which should be more noticeable in the range of maximum absorption.

Since absorption measurement errors are greater in the center of the band, it is possible to decrease the weight of these points in the data treatment using an error model. It gives additional degree of freedom for calculated mixing parameters, but should result in better general agreement between model profile and measurements. Because measurement errors are expected to grow along with the gas absorption, we use the band absorption profile as a base for the error model. To define parameters of the model, three pairs of band-profile records were compared. Each pair consisted of records observed at close temperatures (252 and 253 K, 300 and 303 K, 324 and 327 K). If we take the absolute value of differences between the residual errors of two records, the regular part of the residuals will cancel, and the frequency range where noise increases will be evident (in this case, the residuals between recorded profiles and the absorption model of [10] were taken by reason of the latter's independence from the current recorded profiles). In Fig. 6 the dots show absolute values of the difference between residuals, and the solid line is the noise-model function:

$$E_{exp}(f) = max(\sigma, 0.015 \cdot (\alpha(f) - 12.0)) \tag{8}$$

with $\sigma = 0.01$ dB/km; $\alpha(f)$ in dB/km is calculated at each temperature. At temperatures higher than 310 K, this noise model reduces to the constant level of σ. Then the data are pre-whitened by the factor

$$s_k = E_{exp}(f_k)/\sigma \tag{9}$$

Use of the noise model leads to an increase of the residual in the center of the band but at the same time decreases the residual in the ranges from 53 to 56 GHz and from 63 to 66 GHz, at temperatures below 0 °C, which will be useful for many applications.

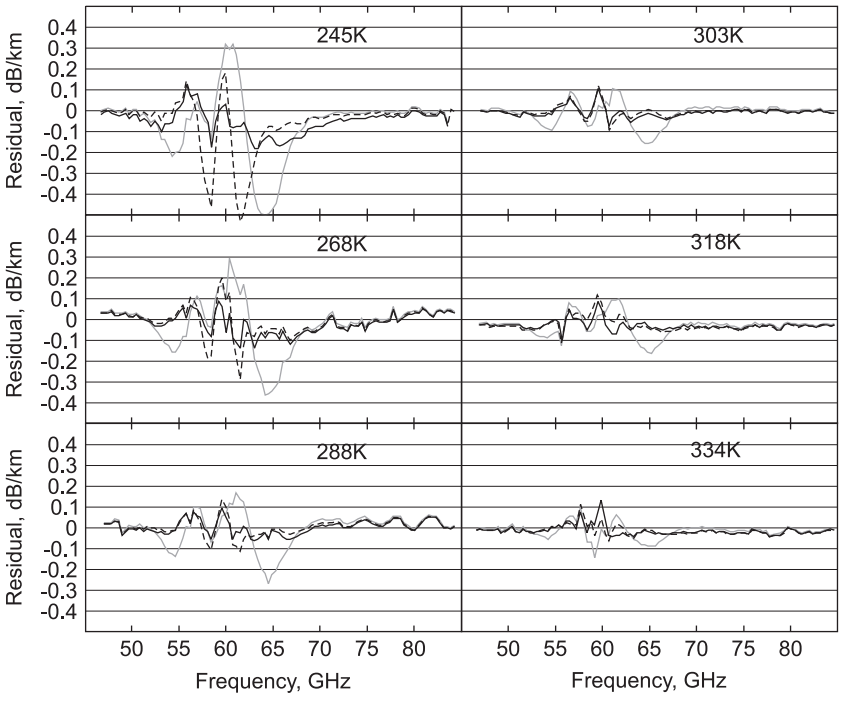

Fig. 5. Experiment-minus-model residual errors at several temperatures, for second-order mixing models fitted to each temperature (black lines), the model of [10] (gray lines), and the model using coefficients from Table 1 (dotted lines).

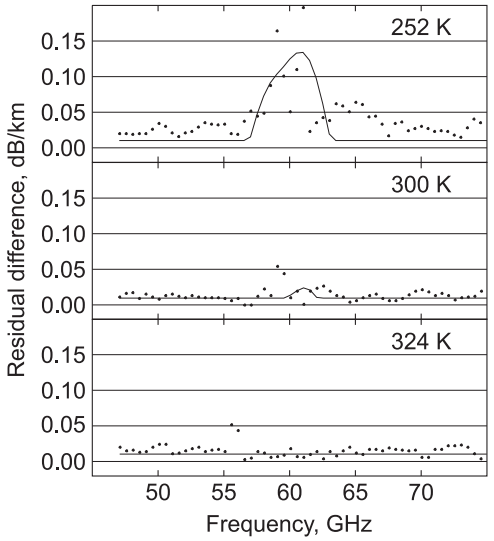

Fig. 6. Absolute value of the close temperature records' residuals difference (points) and error model (solid line).

Measurements were carried out over a wide temperature range, so one should pay attention to temperature dependence of the mixing coefficients. Ref. [9], says that "if the temperature variation in the *Y*'s contains a term that varies with $(300/T)^x$, then for at least some of the coefficients there will also be a term varying with $(300/T)^{x+1}$. This argument does not prove that two terms in powers of $(300/T)$ will always be sufficient to represent the temperature dependence of the Y_k, but at least two are necessary to maintain detailed balance". According to this reasoning, an expression accounting for temperature dependence of mixing coefficients was written as

$$Z_i(T) = \left(Z_i^0 + Z_i^1 \cdot \left(\frac{300}{T} - 1\right)\right) \cdot \left(\frac{300}{T}\right)^x \tag{10}$$

where Z_i is a first- or second-order coefficient y_i, g_i or $\delta\nu_i$, Z_i^0 is the mixing coefficient value at 300 K, and the Z_i^1 term accounts for the $(300/T)^{x+1}$ dependence; $x=0.8$ for y_i (the origin of this value for the temperature exponent is discussed below) and $x=1.6$ for g_i and $\delta\nu_i$. The reason for the difference in x values is the fact that second-order mixing coefficients are proportional to sums of terms involving products of two elements of the collisional-relaxation matrix [7]; while first-order mixing coefficients are proportional to sums of terms involving individual matrix elements.

Our algorithm code for estimation of mixing coefficients produces values reduced to the exponential dependence $(300/T)^x$, thus they should depend on T as $Z_i^0 + Z_i^1 \cdot (300/T - 1)$. As one can see in Fig. 7, the dependence of these values on $(300/T)$ can be considered as linear within the accuracy of estimation. With the second-order mixing effect taken into account, first-order mixing coefficients changed only slightly. Temperature dependences of *y*-coefficients from MPM [10] are shown by the dashed lines in Fig. 7 for comparison.

Table 1 lists the coefficients thus obtained, with pre-whitening applied. Data from the table are presented in

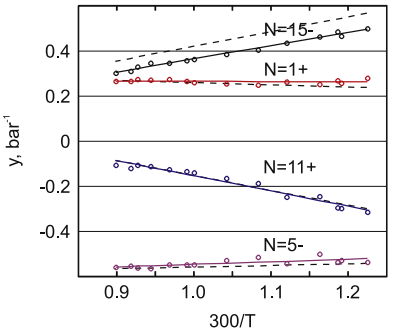

Fig. 7. Reduced first-order mixing coefficients vs. inverse temperature (solid lines), calculated coefficients' values (circles) and reduced first-order mixing coefficients vs. inverse temperature from [10] (dashed lines). The factor $(300/T)^{0.8}$ has been removed from the coefficients.

graphical form in Fig. 8. Other coefficients necessary for computation of absorption can be found in Table 5 of [10].

The value of $x=0.8$ was measured experimentally for broadening of the 9+ line [8] and is still used in MPM and in the current model as a uniform temperature coefficient for all lines, i.e. $\gamma_i = \gamma_i^0 \cdot (300/T)^{0.8}$. In [13] the value of $x=0.785(35)$ (which coincides with $x=0.8$ within experimental uncertainty) was measured for the 1− line. In our earlier work [10] it was shown that broadening coefficients (γ) of the discussed fine-structure lines are very close to ones of the corresponding lines of the A-band (see Fig. 5 in [10]) at room temperature. This fact suggests that temperature coefficients x for corresponding lines in the fine-structure band and A-band might also have close values. Experimentally measured x-coefficients for A-band [18] range from 0.6 to 0.77 and they appear to depend regularly on the quantum number N, so it would be natural to suppose that the 60-GHz absorption band may behave in the same way. We tried to use the temperature coefficients' dependence on N from [18] for line-widths and first-order mixing coefficients in our calculations. It resulted in insignificant differences in residuals and slight differences (about 5%) in derived mixing coefficients, in comparison to using the uniform x value for all lines. Therefore, we decided to keep the uniform value for all lines until new experimental data on the dependence for individual lines is obtained.

The mixing coefficients in Table 1 are the result of fitting the calculated coefficients for each temperature point by Eq. (10), so using coefficients from the table for absorption-band modeling gives residuals which differ from those which were derived by treatment of each isolated record and without pre-whitening. In Fig. 5, the dashed black line plots residuals with the new second-order model using parameters from Table 1. Use of pre-whitening tends to reduce residuals in the band wings, but increase them in the band center (because the weight of measured points in the center of the band was decreased). One notices that residuals in the center of the band, obtained with pre-whitening, look systematic, but their magnitude is not greater than that of systematic residuals given by MPM in the same figure. With decreased residuals in the band wings, this means that systematic errors in reproducing the

Table 1
First- and second-order mixing parameters.

N	y^0, bar^{-1}	y^1, bar^{-1}	g^0, bar^{-2}	g^1, bar^{-2}	$\delta\nu^0$, GHz bar^{-2}	$\delta\nu^1$, GHz bar^{-2}
1−	−0.041[a]	0.000	0.000	0.000	0.000	0.000
1+	0.265	−0.0132	−0.0835	0.00843	0.00545	0.0017
3−	−0.354	0.0582	−0.0947	0.0234	−0.0175	−0.0013
3+	0.53	−0.0981	−0.218	0.0596	0.0286	0.00107
5−	−0.547	0.114	−0.16	0.0326	−0.043	−0.00444
5+	0.589	−0.153	−0.162	0.041	0.0491	0.00493
7−	−0.359	−0.0494	0.0197	0.0174	−0.0229	−0.0529
7+	0.276	0.0476	0.132	0.039	0.0162	0.061
9−	−0.0942	0.186	0.128	0.262	−0.000866	−0.0193
9+	−0.0124	−0.235	0.166	0.305	−0.00609	0.0168
11−	0.0647	0.611	0.0883	0.126	−0.00115	0.0393
11+	−0.155	−0.674	0.0713	0.0799	−0.00256	−0.0448
13−	0.224	0.628	0.0735	−0.156	0.00221	0.0247
13+	−0.299	−0.662	0.0582	−0.216	−0.00447	−0.0265
15−	0.365	0.583	−0.00369	−0.253	0.00605	0.0102
15+	−0.426	−0.598	0.00439	−0.296	−0.00746	−0.0106
17−	0.466	0.596	−0.0213	−0.287	0.00675	0.0104
17+	−0.515	−0.6	−0.0634	−0.324	−0.00762	−0.0105
19−	0.546	0.617	−0.0868	−0.374	0.00732	0.0163
19+	−0.587	−0.615	−0.105	−0.394	−0.00784	−0.0163
21−	0.608	0.515	−0.114	−0.393	0.00802	0.00835
21+	−0.642	−0.509	−0.134	−0.4	−0.00833	−0.00815
23−	0.64	0.406	−0.163	−0.329	0.00696	0.000922
23+	−0.668	−0.399	−0.174	−0.328	−0.00714	−0.00076
25−	0.655	0.348	−0.186	−0.261	0.00517	−0.00174
25+	−0.679	−0.34	−0.195	−0.258	−0.00526	0.00184
27−	0.669	0.335	−0.179	−0.237	0.00368	−0.0015
27+	−0.689	−0.327	−0.186	−0.232	−0.00376	0.00157
29−	0.689	0.342	−0.184	−0.244	0.00277	−0.000561
29+	−0.706	−0.332	−0.189	−0.239	−0.00283	0.000641
31−	0.715	0.346	−0.197	−0.262	0.0023	−0.0000939
31+	−0.729	−0.336	−0.2	−0.254	−0.00235	0.000173
33−	0.743	0.344	−0.212	−0.278	0.00209	−0.0000366
33+	−0.754	−0.334	−0.214	−0.268	−0.00211	0.000099
35−	0.771	0.338	−0.227	−0.295	0.00194	−0.000156
35+	−0.78	−0.327	−0.228	−0.283	−0.00197	0.000224
37−	0.802	0.32	−0.215	−0.354	0.00199	−0.000708
37+	−0.807	−0.309	−0.216	−0.336	−0.00199	0.000743

[a] Value from [13].

experimental data by means of the new second-order mixing model are in general better than those of MPM. Modeling the temperature dependence of the coefficients with an analytic function Eq. (10) leads to increased residuals generally, since the function does not reproduce each temperature exactly. But since measurement errors in the center of the band are most likely related to the fluctuation of the oxygen concentration, they should be considered as statistical, not systematic. Fitting an analytical temperature dependence to the mixing coefficients is a form of averaging, which is known to reduce the statistical errors. Hence, even if the accuracy of reproducing the experimental profiles seems to be reduced, there is a reason to believe that it actually is beneficial. One also notices that the modeled second-order mixing still leaves some systematic residuals at the band wings. This might be due to limitations of the model, such as neglecting of mixing between the $N+$ and $N-$ branches, or to underestimated temperature dependence of the lines' collisional parameters, as discussed in the previous paragraph. However, as shown in Fig. 9, between 54 and 65 GHz, the residuals using coefficients from Table 1 are on the order of 2% or less of the measured absorption at each frequency.

We would like to point out some possible experimental improvements which could further improve the accuracy of the band absorption-profile modeling. (We do not discuss here improvement of the spectrometer sensitivity, which obviously leads to that goal but it is not easily attainable.) The first would be to use artificial air having a known concentration of oxygen and nitrogen instead of outdoor air. This would avoid the trouble with oxygen concentration mentioned in the experimental section. The second improvement could be direct measurement of temperature dependence of individual line-broadening coefficients. That can be done at low pressures using a spectrometer with radio-acoustic detection [10] additionally equipped with a temperature-regulated thermostat for the absorption cell.

5. Comparison with other work

Line mixing has the proportionately greatest effect on the wings of a band. Therefore, measurements at frequencies

higher than those from which the new model was derived are a stringent test of its accuracy. At frequencies far from the main resonances, absorption in dry air is dominated by the collision-induced absorption by nitrogen, so measurements of pure oxygen provide a better test of an oxygen-band model. Fig. 10 shows a comparison to the pure-oxygen measurements from Fig. 11 of [19]. The air model's predicted absorption has been scaled upward by a factor of 4.774, ignoring possible differences in broadening and mixing coefficients between air and pure O_2. The calculation included the contribution from a weak $^{16}O^{18}O$ line at 234 GHz. We used a half-width value of 2.8 GHz/bar for this line, taken from [19], although it is 68% larger than another recent measurement of that line [20]. The "total" curve also includes O_2–O_2 collision-induced absorption, based on the work in [21]. Absorption due to the submillimeter rotational lines of O_2 is barely significant in the plotted frequency range; however, it is included in the total also.

Although we would not vouch for the accuracy of the model at three atmospheres, it is in fair agreement with the data in Fig. 10. It is worth mentioning that the contribution of the non-resonant or Debye component of the oxygen spectrum in Fig. 10 is 0.065 km^{-1}; the total absorption is less than this value as a consequence of the mixing-coefficient biases b_i, which account for mixing between the resonant and non-resonant branches. This effect is confirmed by the measurements of [19], which also are below the Debye value over most of this frequency range.

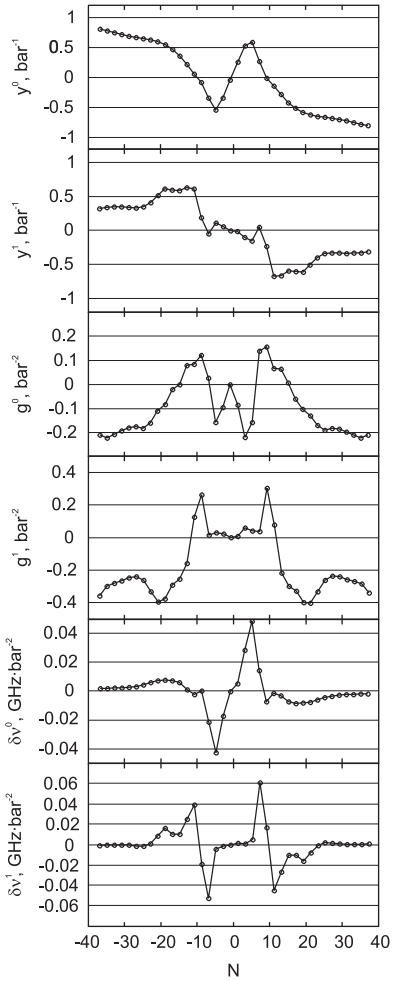

Fig. 8. Mixing coefficients from Table 1.

6. Conclusions

Improvements of the resonator spectrometer and the method of measurement presented in [13,14] as well as algorithm extensions in the present work permitted a refined analysis of the 60-GHz atmospheric oxygen

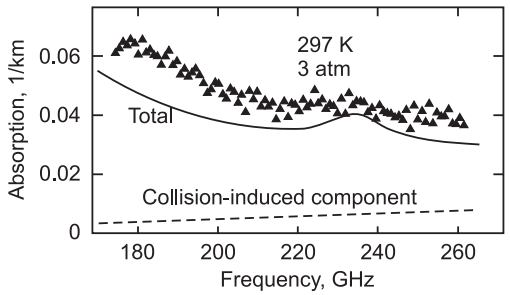

Fig. 10. Power absorption coefficient in pure oxygen at 3 atm. Measurements from [19] (triangles), calculation based on the discussed second-order mixing model (solid line), collision-induced absorption (dashed line).

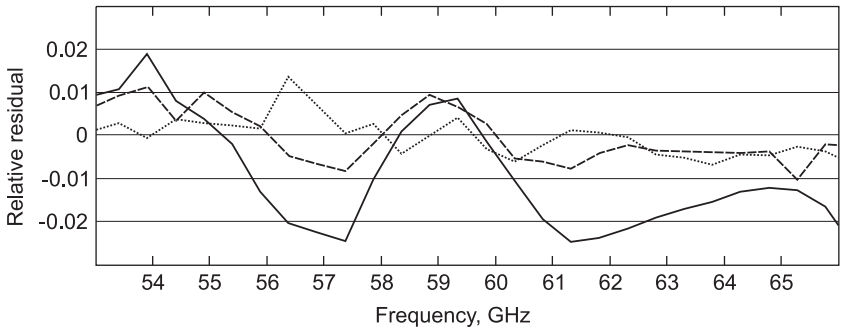

Fig. 9. Residuals between recorded profiles and second-order model using coefficients from Table 1, relative to the measured absorption value, at three temperatures: 245 K (solid line), 288 K (dashed line) and 334 K (dotted line). The highest, the lowest and the central temperature of the measured temperature range are chosen for the figure.

absorption band. Precise experimental data on the band profile were obtained at pressures near one atmosphere in the temperature range of 245–334 K, which covers a substantial part of the Earth's atmospheric temperature range. The second-order mixing effect was taken into account for experimental data processing, and first- and second-order mixing coefficients were derived. The mixing coefficients' dependences on temperature and on quantum number are consistent with earlier data and theoretical predictions. Between 54 and 65 GHz, residual errors between the extended model and the observed absorption profiles are typically 2% or less, which is an improvement on MPM.

The information obtained in the course of this work can be applied to Earth-atmosphere remote sensing, microwave wireless communication, and industrial applications, as well as for fundamental spectroscopic studies.

Acknowledgment

The work presented in this paper was supported in part by the Russian Foundation for Basic Research.

References

[1] van Vleck JH, Weisskopf VF. On the shape of collision-broadened lines. Rev Mod Phys 1945;17:227–36.
[2] van Vleck JH. Magnetic dipole radiation and atmospheric absorption bands of oxygen. Astrophys J 1934;80:161–70.
[3] vanVleck JH. The absorption of microwaves by oxygen. Phys Rev 1947;71:413–24.
[4] Baranger M. Problem of overlapping lines in the theory of pressure broadening. Phys Rev 1958;111(2):494–504.
[5] Fano U. Pressure broadening as a prototype of relaxation. Phys Rev 1963;131(1):259–68.
[6] Rosenkranz PW. Shape of the 5 mm oxygen band in the atmosphere. IEEE Trans Antennas Propagat 1975;23(4):498–506.
[7] Smith EW. Absorption and dispersion in the O_2 microwave spectrum at atmospheric pressures. J Chem Phys 1981;74(12):6658–73.
[8] Liebe HJ. MPM—an atmospheric millimeter-wave propagation model. Int J Infrared Mill Waves 1989;10:631–50.
[9] Liebe HJ, Rosenkranz PW, Hufford GA. Atmospheric 60 GHz oxygen spectrum: new laboratory measurement and line parameters. J Quant Spectrosc Radiat Transfer 1992;48(5–6):629–43.
[10] Tretyakov MY, Koshelev MA, Dorovskikh VV, Makarov DS, Rosenkranz PW. 60 GHz oxygen band: precise broadening and central frequencies of fine structure lines, absolute absorption profile at atmospheric pressure, revision of mixing coefficients. J Molec Spectrosc 2005;231:1–14.
[11] Rothman LS, Jacquemart D, Barbe A, Benner DC, Birk M, Brown LR, et al. The HITRAN 2004 molecular spectroscopic database. J Quant Spectrosc Radiat Transfer 2005;96:139–204.
[12] Rosenkranz PW. Interference coefficients for overlapping oxygen lines in air. J Quant Spectrosc Radiat Transfer 1988;39:287–97.
[13] Makarov DS, Koval IA, Koshelev MA, Parshin VV, Tretyakov MY. Collisional parameters of the 118 GHz oxygen line: temperature dependence. Journal of Molecular Spectroscopy 2008;252:242–3.
[14] Tretyakov MY, Krupnov AF, Koshelev MA, Makarov DS, Serov EA, Parshin VV. Resonator spectrometer for precise broadband investigations of atmospheric absorption in discrete lines and water vapor related continuum in millimeter wave range. Rev Sci Instrum 2009;80:093106-1–0.
[15] Kogelnik H, Li T. Laser beams and resonators. Appl Opt 1966;5(10):1550–67.
[16] Lam KS. Application of pressure broadening theory to the calculation of atmospheric oxygen and water vapor microwave absorption. J Quant Spectrosc Radiat Transfer 1977;17:351–83.
[17] Rosenkranz PW. Retrieval of temperature and moisture profiles from AMSU-A and AMSU-B measurements. IEEE Trans Geosci Remote Sensing 2001;39(11):2429–35.
[18] Brown LR, Plymate C. Experimental line parameters of the oxygen A-band at 760 nm. J Mol Spectrosc 2000;199:166–79.
[19] Meshkov AI, Lucia FCD. Laboratory measurements of dry air atmospheric absorption with a millimeter wave cavity ringdown spectrometer. J Quant Spectrosc Radiat Transfer 2007;108(2):256–76.
[20] Drouin BJ. Temperature dependent pressure induced linewidths of and $^{18}O^{16}O$ transitions in nitrogen, oxygen and air. J Quant Spectrosc Radiat Transfer 2007;105(3):450–8.
[21] Boissoles J, Boulet C, Tipping RH, Brown A, Ma Q. Theoretical calculation of the translation-rotation collision-induced absorption in N_2–N_2, O_2–O_2, and N_2–O_2 pairs. J Quant Spectrosc Radiat Transfer 2003;82(1–4):505–16.